NATIONAL ADVISORY COMMITTEE FOR AERONAUTICS

TECHNICAL NOTE

No. 1781

COMPARISON OF OVER-ALL IMPACT LOADS OBTAINED DURING SEAPLANE LANDING TESTS WITH LOADS PREDICTED BY HYDRODYNAMIC THEORY

By Margaret F. Steiner

Langley Aeronautical Laboratory
Langley Field, Va.

Washington
January 1949

NATIONAL ADVISORY COMMITTEE FOR AERONAUTICS

TECHNICAL NOTE NO. 1781

COMPARISON OF OVER-ALL IMPACT LOADS OBTAINED DURING SEAPLANE LANDING TESTS WITH LOADS PREDICTED BY HYDRODYNAMIC THEORY

By Margaret F. Steiner

SUMMARY

A landing investigation was conducted with a flying boat having a conventional configuration to determine the applicability of hydrodynamic impact theory in defining full-scale water impact loads.

The loads and displacements obtained in landings of a full-scale flying boat in smooth water in which little rotation in pitch occurred and in which only the V-shape portion of the forebody was involved were in good agreement with computed values based on general hydrodynamic impact theory.

In the majority of the normal landings, the chines were immersed in the free water surface at the time of maximum load. Because of the lower dead rise on the curved-chine region, the local pressures on that region were considerably higher than on the main plating, which had an angle of dead rise of 20°. The resultant maximum loads for all cases of chine immersion were about 60 percent greater than those computed for a V-shape prismatic body having an angle of dead rise of 20° with no allowance being made for transverse curvature near the chines.

In those impacts in which the aircraft rotated to a lower trim with a fairly large angular velocity, the experimental loads in the early portion of the impact in which only the V-shape portion of the forebody was involved were considerably less than the computed loads, but there was no corresponding reduction in maximum load.

The wetted semibeam was found to be approximately 40 percent greater than the semibeam in the plane of level water.

INTRODUCTION

In an endeavor to predict adequately the values of hull load to be used in the design of modern water-based aircraft, a hydrodynamic impact theory (references 1 to 4) has been developed and verified with data from controlled impact-basin tests for a V-shape prismatic body entering the water with fixed trim for a wide range of angles of trim, dead rise, and flight path.

Flight tests of an amphibian-type flying boat were made in order to determine the applicability of the theory to the case of the conventional full-scale airplane. Landings were made in calm water for a range of angles of trim and flight path as wide as practicable.

The measured resultant loads and displacements are compared with those computed on the basis of the impact theory and general observations are made about certain measured quantities such as wing lift. No attempt is made to determine quantitatively the effects of all the factors that deviate from the simplified case of the immersing wedge which was used in the derivation of the impact theory. The effects of variation of trim during impact and transverse curvature near the chine are discussed.

The measured wetted widths are compared with the width of the float in the plane of level water and the ratio of these two quantities is compared with the effective growth in beam which has been discussed in previous papers concerning the hydrodynamic impact theory.

SYMBOLS

b beam in plane of level water

C_l load-factor coefficient $\left(\frac{n_{i_w} g}{V_{v_o}^2}\left(\frac{W}{g}\left\{\frac{6 \sin \tau \cos^2 \tau}{[f(\beta)]^2 \phi(A) \rho \pi}\right\}\right)^{1/3}\right)$

C_d draft coefficient $\left(y\left(\frac{g}{W}\left\{\frac{[f(\beta)]^2 \phi(A) \rho \pi}{6 \sin \tau \cos^2 \tau}\right\}\right)^{1/3}\right)$

C_t time coefficient $\left(tV_{v_o}\left(\frac{g}{W}\left\{\frac{[f(\beta)]^2 \phi(A) \rho \pi}{6 \sin \tau \cos^2 \tau}\right\}\right)^{1/3}\right)$

c wetted semiwidth

g acceleration due to gravity, 32.2 feet per second per second

l wetted length along keel

n_{l_w} impact load factor normal to water surface $\left(\frac{d^2y/dt^2}{g}\right)$

t time after contact, seconds

V_h horizontal velocity of seaplane relative to water, feet per second

V_v vertical velocity of step relative to water, feet per second

W weight of seaplane, pounds

y draft normal to water surface, feet

z penetration of a given station, normal to keel

$f(\beta)$ dead-rise correction to water mass $\left(\frac{\pi}{2\beta} - 1;\ \beta \text{ expressed in radians}\right)$

$\phi(A)$ end-loss correction to total hydrodynamic load $\left(1 - \frac{\tan \tau}{2 \tan \beta}\right)$

β angle of dead rise, degrees

γ flight-path angle, degrees $\left(\tan^{-1} \frac{V_v}{V_h}\right)$

κ approach parameter

ρ mass density of water, $\frac{63.5}{32.17}$ pound-seconds^2 per foot^4

τ trim, degrees

τ_p trim at time of maximum load, degrees

ω pitching velocity, degrees per second

Subscripts:

A pertaining to instant at which water line reached curved-chine region

D pertaining to instant at which water line reached chine

F pertaining to instant at which water line intersected keel in plane LL' (See appendix B.)

max maximum

o at time of water contact

THE AIRPLANE AND INSTRUMENTATION

The airplane used in the hydrodynamic load investigation was the amphibian-type flying boat pictured in figure 1. Pertinent information about the airplane is given in table I and the hull lines are shown in figure 2.

Extensive instrumentation was employed to obtain trim, vertical velocity, horizontal velocity, acceleration at the center of gravity, wetted bottom area, and local water pressures on the hull bottom.

The relative location of the instrumentation in the flying boat used in the investigation of the over-all load is shown in figure 3. The specific locations are given in tables II, III, and IV.

The horizontal component of the speed of the airplane relative to the water was determined from measurements of the hydrodynamic head with an inductive-type water-speed pressure gage which was mounted at the same level as the keel near the forebody step as shown in figure 4(a). The airspeed, which is of help in defining the type of approach, was obtained with an NACA airspeed recorder mounted above the pilot's compartment as shown in figure 4(b). The time history of the trim was obtained with a gyroscopic recorder which was mounted in the floor of the cabin as shown in figure 4(c).

The vertical velocity of the forebody step relative to the water surface at time of contact with the water was the most difficult variable to measure. A small 16-millimeter motion-picture camera was mounted near the tip of the wing, as shown in figure 4(d), so that it was focused on the region around the forebody step where a retractable rod 3 feet in length (vertical-displacement indicator) was installed as shown in figure 4(e). The exact procedure followed in obtaining the vertical velocity through the use of these devices is explained in appendix A.

The acceleration of the center of gravity measured normal to the keel was obtained with two accelerometers. One was an NACA optical-recording three-component accelerometer having a natural frequency of the vertical component of about 19 cycles per second. The second instrument was an inductive-type accelerometer having a natural frequency of about 40 cycles per second. Both accelerometers were mounted rigidly near the center of gravity as shown in figure 4(f).

The wetted bottom areas were determined by the inspection of records showing time of immersion of various pressure gages and water contacts which were located along the bottom as shown in figure 5. The flush-mounted diaphragms of two pressure gages may be seen in figure 4(a). The water contacts, which are not shown in this figure, were small spark plugs which were adapted so as to cause a small

neon bulb to light when water passed over a plug and closed the electric circuit through each plug. The wetted lengths used in conjunction with the corresponding instantaneous values of trim provided the time history of the vertical displacement of the step below level water.

The amplifying and recording equipment used with the pressure gages, the inductive-type accelerometer, the NACA airspeed recorder, the water-speed pressure gage, and the frame counter for the wing camera is shown in figure 6.

PRECISION OF MEASUREMENTS

The following values are estimated accuracies of reported experimental data based on both instrument and reading error:

V_h, percent	±4
V_v, percent	±10
τ, degrees	±0.25
n_{i_w}, percent	±10
y, feet	±0.03
Wing lift, multiples of airplane weight	±0.05
Pressure, pounds per square inch	±1

THEORY AND METHOD OF APPLICATION

Impact Theory

The loads on V-bottom seaplanes have been analyzed for simplified conditions in references 1 and 2. In these references it was assumed that: (a) the trim remained fixed, (b) the prismatic V-section was sufficiently long so that the pulled-up-bow region, which is indicated in figure 2, did not enter the water, and (c) the wing lift was equal to the weight of the airplane. With these assumptions it was shown that the loads and motion of the seaplane could be represented in generalized form by means of the following dimensionless variables:

Load-factor coefficient

$$C_l = \frac{n_{i_w} g}{V_{v_o}^2}\left(\frac{W}{g}\left\{\frac{6 \sin \tau \cos^2 \tau}{\left[f(\beta)\right]^2 \phi(A) \rho \pi}\right\}\right)^{1/3}$$

Draft coefficient

$$C_d = y\left(\frac{g}{W}\left\{\frac{[f(\beta)]^2\phi(A)\rho\pi}{6 \sin \tau \cos^2\tau}\right\}\right)^{1/3}$$

Time coefficient

$$C_t = tV_{v_o}\left(\frac{g}{W}\left\{\frac{[f(\beta)]^2\phi(A)\rho\pi}{6 \sin \tau \cos^2\tau}\right\}\right)^{1/3}$$

These nondimensional coefficients were shown to be related to each other at all instants during an impact by the approach parameter κ, which is dependent upon the initial conditions of trim and flight path, where $\kappa = \frac{\sin \tau \cos(\tau + \gamma_o)}{\sin \gamma_o}$. For a given value of κ, the variation of each of these coefficients with any other was represented by a single curve. The variations of C_d and C_l with C_t, as taken from reference 2, are shown in figure 7. Thus, for any angle of dead rise, angle of trim, or vertical velocity, impacts having the same value of κ were shown to have time histories which were mathematically similar. Each value of κ, however, identifies a different time-history shape. The absolute values of draft, time, and acceleration, which may be obtained from the dimensionless coefficients, are dependent upon the geometric properties of the seaplane, the weight, the initial vertical velocity, and so forth.

It was also shown that variation of the maximum values of the load-factor coefficient with the approach parameter κ could be represented by a single theoretical curve and that all experimental data for the conditions which were represented in impact-basin tests lay along this curve for a wide range of test conditions. This curve is the heavy-line curve in figure 8.

Application of Theory to Flight Data

The cross section of the hull bottom as shown in the line drawing of figure 2 was a V-section at the keel with transverse curvature near the chine. In the treatment of transverse curvature of a scalloped-bottom float which was presented in reference 3, a theoretical method was presented for calculating the loads on curved bottoms. However,

it was felt that the additional complexity introduced by consideration of transverse curvature was not warranted in the present investigation. As a result, the effects of chine flare on the maximum total loads are neglected and a constant dead-rise angle of 20° is used throughout the analysis. In addition, the beam is assumed to be infinitely large, so that the chine is not considered to be immersed.

Water Pile-Up

One factor that is of interest in the application of the theory to the actual seaplane is the transverse water pile-up that appears in the case of an immersing float. In reference 2, which is concerned with a straight-side V-bottom, this pile-up was interpreted as being an effective growth in width in which the wetted width $2c$ was equal to the product of the ratio $\frac{\frac{\pi}{2\beta} - 1}{\cot \beta}$ and the beam in the plane of level water. The determination of the actual pile-up is desired in that it defines the area upon which the load acts. The actual growth of width which was obtained by analyzing the measured wetted areas is compared in the section entitled "Measured Water Pile-Up" with the effective growth as indicated by the theoretical impact equations. The comparison is arbitrarily made on the basis of depth dimensions rather than width.

TEST PROCEDURE

Landings were made in calm water and the measured approach variables at time of water contact for the impacts analyzed in this report are given in table V. As noted in the last column, these impacts were frequently the second or third impact during a landing.

The center-of-gravity accelerations measured with the NACA optical-recording three-component accelerometer are given as faired values in figure 9; the actual record had oscillations similar to those recorded by the inductive-type accelerometer. The acceleration value at time of forebody contact was used as a reference, and any subsequent variation from that value was interpreted as being due to the water load.

RESULTS AND DISCUSSION

The data are presented in the form of maximum nondimensional load-factor coefficients which vary with the approach parameter κ as shown in figure 8. The corresponding values of the variable used in computing the maximum load-factor coefficients for the actual impacts

are given in table VI. The data are assorted as to type of impact; that is, whether only the V-shape portion of forebody is involved, whether the chine is immersed, or whether the bow region or the afterbody is involved.

Typical time histories of experimental loads and drafts as compared with computed time histories based on figure 7 are given in figure 9.

The approximate instant of bow immersion, chine immersion, and so forth are indicated by letters on the figures as follows:

A water pile-up reaches curved-chine area; $y = y_A = 0.73$ feet

B pulled-up-bow region enters water; wetted length is 156 inches

C level water passes chine; $y = 1.17$ feet

D water pile-up reaches chine; $y = y_D = 0.9$ feet

E point of application of force reaction is under center of gravity

The values of y_A and y_D which are listed are based on the relationship between actual draft and the wetted depth which was determined by the method explained in appendix B. The water pile-ups as determined for a number of impacts for which accurate wetted areas were available are listed in table VII.

Chine above Level Water at Time of Peak Load

The first results which are discussed are those from impacts which most nearly represented the simplified case upon which the theory is based; namely, forebody impacts in which only the prismatic portion was involved at time of peak hydrodynamic load. Such impacts are represented in figure 8 by the circles. Good agreement between experimental points and the theoretical curve for the maximum load factor exists for this condition. This agreement is further illustrated by the time histories of the experimental and computed loads (figs. 9(a) and 9(b)) for two impacts in which the maximum load factor was reached prior to chine immersion. The time histories, for most impacts, show that the experimental values of the load are slightly less than the computed values in the early stages of the impacts. This difference can probably be attributed largely to the fact that the trim of the airplane decreased during the impact. The effect of the variation of trim on the loads is discussed in detail in a subsequent section.

Chine Immersed at Time of Peak Load

Region of forebody having constant cross section involved.- Although most of the landings were comparatively light (see table VI), it was observed that the chine usually became immersed prior to time of peak load. During some impacts of this type only the portion of the forebody having constant cross section was involved at time of peak load. Such impacts are represented in figure 8 by the squares without flags. Impacts in which the afterbody was involved at time of forebody contact but was not involved at time of peak load are represented in figure 8 by squares having flags.

For impacts of these types the maximum experimental loads are always greater than the computed loads, the approximate mean of experimental values (as indicated by the dash-line curve) being about 60 percent higher than the theoretical curve. The time histories given in figures 9(c), 9(e), 9(g), 9(h), and 9(i) show that the experimental and computed loads were in good agreement until the water line reached the curved-chine region. After this time, the reaction moved forward of the center of gravity and the load increased and exceeded the corresponding computed values based on a V-shape cross section with no transverse curvature. This increase in load is attributed principally to the high local pressures (due to the lower local dead rise) on the curved-chine region; these pressures exceed those on the adjacent region nearer the keel. This is evidenced in the presentation in figure 10 of typical pressure distributions which were based on pressures measured during run 15.

Pulled-up-bow region of forebody involved.- In two extreme cases the trim and displacement were such that the pulled-up-bow region was involved before peak load was reached. The immersion of the bow has two distinct effects on the total load. Because of the pulled-up section, the actual wetted length in the plane of the water surface after the water line reaches the bow region is less than that which would be obtained if the hull were completely prismatic and the keel continued forward indefinitely in a straight line. This reduction in wetted length would tend to make the load after bow immersion somewhat less than that predicted by the theory for a prismatic form. This reduction is, however, somewhat offset by the increased local trim of the bow region so that the load would tend to be increased.

These impacts are represented in figure 8 by the triangles, and their time histories are shown in figures 9(d) and 9(f). In these impacts the experimental peak load was less than the computed load. In run 22, which is presented in figure 9(d), the effect of the pulled-up bow in reducing the peak load is indicated as the curved-chine region did not become appreciably involved until after time of peak load.

Effect of Angular Rotation during Impact

The step of the airplane used in the tests was located about 30 inches aft of the center of gravity so that the reaction remained aft of the center of gravity until a forebody wetted length of about 90 inches was reached, since the center of pressure is approximately one-third of the wetted length forward of the step. (See reference 5.) The instant at which the point of application of the force reaction was under the center of gravity is indicated on the abscissa of figure 9 by the letter E. Because of the location of the step relative to the center of gravity of the airplane, the airplane rotated downward after water contact.

Downward rotation caused a reduction in load in the early part of the impact (before the chine-flare region became immersed) because of the decrease in trim which results in smaller water loads, but there was no corresponding reduction in maximum load. The effect of rotation was most noticeable in high-trim impacts in which the afterbody contacted the water before the forebody, so that high angular diving velocities were present at the time of forebody contact. There was a reduction in load in the early part of such an impact as compared to an impact which had no angular velocity, as can be seen from a comparison of figures 9(j) and 9(i). The reduction in load during the early part of the impact permitted the hull to immerse more deeply than if the airplane had remained at fixed trim, and so the chine flare was immersed at a vertical velocity only slightly less than the initial value. This fact is evidenced in the nearly linear displacement curves of figure 9 up to $y = y_A$ (the point at which the water pile-up reached the curved-chine area). As a result of the high vertical velocities which existed when the water surface reached the chine-flare region with its lower dead rise, high local pressures were attained in the region of transverse curvature and the measured maximum loads were always greater than the loads computed for fixed-trim impacts on the basis of a straight-side V-shape cross section. This result was obtained regardless of the relative magnitude of the pitching velocity at the time of forebody impact.

It can be determined from figure 8 and the data of tables V and VI that the two squares with flags that lie closest to the computed curve are those for the impacts having the highest angular rotation, approximately 16 radians per second, that those lying the farthest from the line of calculated values have angular velocities of between 8 and 11 radians per second, and that the remaining points lie in between the two limits. In all computations the trim at time of forebody contact was used. If the trim at time of maximum load were used in computing the maximum load factor, it is seen by the two typical transposed points in figure 8 that the points representing impacts with highest angular rotation (the points represented by squares with flags closest to the theoretical curve) move closer to the dashed line drawn through the squares that represent impacts having lowest angular rotation in which the trim does not change appreciably before maximum load is reached, whereas the group of points lying farthest from the curve moves even farther from the curve.

The accuracy of the test data and the limited number of runs available are not sufficient to permit the experimental determination of the relationship between the magnitude of the angular velocity and the maximum load.

Measured Water Pile-Up

The effective wetted width which occurs in a transverse plane is given by the impact equations as follows:

$$2c = \frac{\frac{\pi}{2\beta} - 1}{\cot \beta} b$$

If this equation is used for predicting pile-up for an angle of dead rise of 20°, the growth in beam and the corresponding growth in depth due to piled-up water is found to be 27 percent. As observed in table VII, which presents actual measured pile-ups, the average measured wetted width was of the order of 40 percent greater than the beam in the level water surface on the part of the plating having an angle of dead rise of 20°. The accuracy of measurements in a flight test does not permit any exact determination of the effect of pile-up on the total load, so that the value 40 percent has no known relationship with total load but has been presented since such information is useful in defining the plating upon which a given load acts. The pile-up on the curved-chine region with its lower angles of dead rise would be expected to be greater than 40 percent. However, as seen in table VII, the pile-up at the time the water line passes the chine is also about 40 percent. The significance of this is not clear since the actual behavior of the water line between the time it passed gage 16, which was on the outer edge of the V-shape portion of the hull, and the time it reached the chine could not be determined since no pressure gages were placed in that region. The apparent water line near the chine as determined by the peak pressure on gage 17 may have been affected by the discontinuity at the chine and the accompanying end losses which would affect the pile-up at the chine.

Effect of Wing Lift

In table VI it is noted that for a majority of the impacts the float is actually accelerating downward at time of water contact so that the apparent lift on the wing is as low as two-thirds of the weight of the aircraft. No significance has been attached to this fact with regard to resultant load variation since the effects of chine flare and rotation in pitch upon the load appear to be the same regardless of the amount of wing lift at contact.

SUMMARY OF RESULTS

1. The experimental maximum loads obtained in impacts which involved only the V-shape portion of the forebody and in which the aircraft experienced little change in trim were in good agreement with computed values obtained from the application of general hydrodynamic theory.

2. Experimental time histories of loads and displacements for those parts of the impacts in which only the V-shape portion of the forebody was involved were in reasonable agreement with theory for all impacts except those in which high initial angular velocities were present at time of water contact such as in forebody impacts following an initial contact of the afterbody.

3. In the impacts in which the forebody chine was immersed in the free water surface at time of peak load, the experimental peak loads were about 60 percent higher than the computed values which did not take into consideration the effect of the gradual transverse curvature near the chines.

4. In impacts in which the nonprismatic-bow region was involved before peak load was reached, the experimental maximum load was less than the computed load.

5. Downward rotation caused the following effects:

(a) Reduction in load during the early part of an impact but no corresponding reduction in the maximum load.

(b) The reduction in load during the early stages resulted in a greater penetration of the hull and delayed the reduction of the vertical velocity of the aircraft so that the chine flare was immersed at a vertical velocity only slightly less than the initial value. This resulted in high local pressures in the region of transverse curvature, so that the maximum measured loads were greater than the computed loads.

6. Limitations in the test data did not permit the experimental determination of the relationship between the magnitude of the angular velocity and the maximum load.

7. No significance has been attached, with regard to resultant loa variation, to the fact that the wing lift was as low as two-thirds the weight in some impacts since the effects of chine flare and rotation ir pitch upon the load appear to be the same regardless of the amount of wing lift at contact.

8. The measured wetted width was approximately 40 percent greater than the beam in the plane of level water.

CONCLUDING REMARKS

In addition to chine flare and angular rotation, there are many other factors that may affect the over-all load, including elasticity effects, sustained pressures on area behind the intersection of the chine with the water (this is neglected in impact theory), and the effect of variation of wing lift during impact. Nevertheless, when the flight conditions correspond to those for which the theory that neglects these factors was developed, the agreement between experimental and calculated results appears good.

Langley Aeronautical Laboratory
National Advisory Committee for Aeronautics
Langley Field, Va., September 14, 1948

APPENDIX A

PROCEDURE FOR OBTAINING INITIAL VERTICAL VELOCITY

With the aid of the film record, measurements normal and parallel to the forebody keel line were made of the distance from the point of intersection of the rod with the water surface to a reference cross on the side of the flying boat as shown in the sketch:

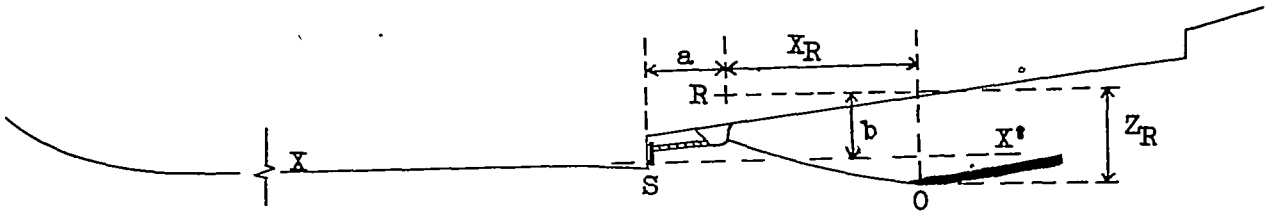

where

a = 1.1 feet

b = 1.35 feet

R	reference point
S	point of step
XX'	keel reference line
Z_R and X_R	distances measured normal and parallel to keel reference line, respectively
O	intersection of rod with water surface

The measured values X_R and Z_R are then referred to the point of the step, so that, as shown in the following sketch,

$$X_S = X_R + 1.1 \tag{1}$$

and

$$Z_S = Z_R - 1.35 \tag{2}$$

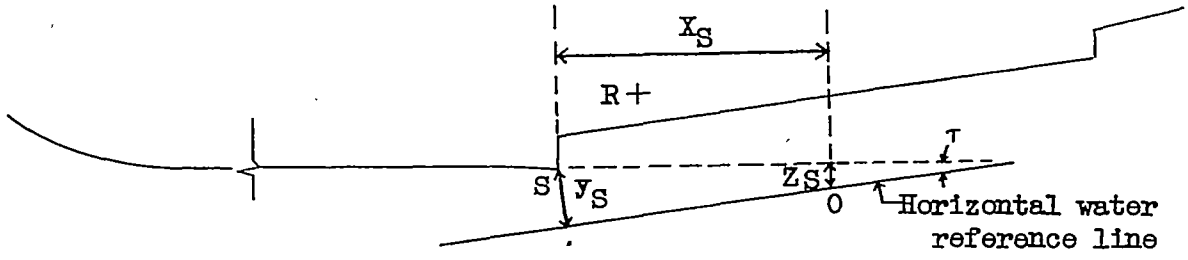

The time history of the actual displacement of the step normal to the water surface y_S before contact of the step with the water may be obtained from the measured time history of the trim since

$$y_S = X_S \sin \tau + Z_S \cos \tau \qquad (3)$$

If the flying boat maintained constant trim before contact, the resultant displacement as obtained from the camera record was usually linear as shown in the following sketch:

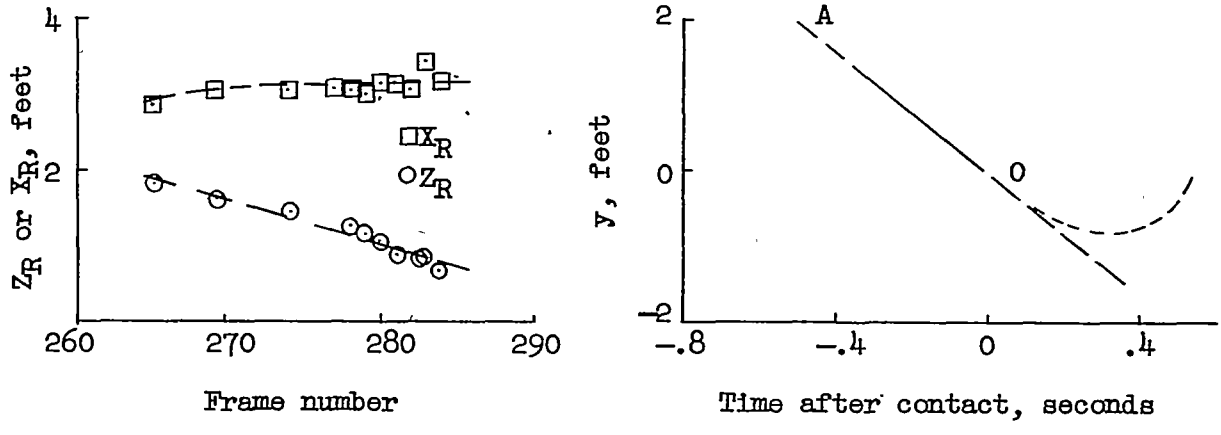

In this case the vertical velocity at contact, which is the slope of the line OA, could be determined with reasonable accuracy, within 5 percent. The small dashed line is the displacement after contact with the water which was obtained from the time histories of the wetted length and trim.

However, for a second impact, a flared landing in which the aircraft changed trim, the resultant displacement was nonlinear:

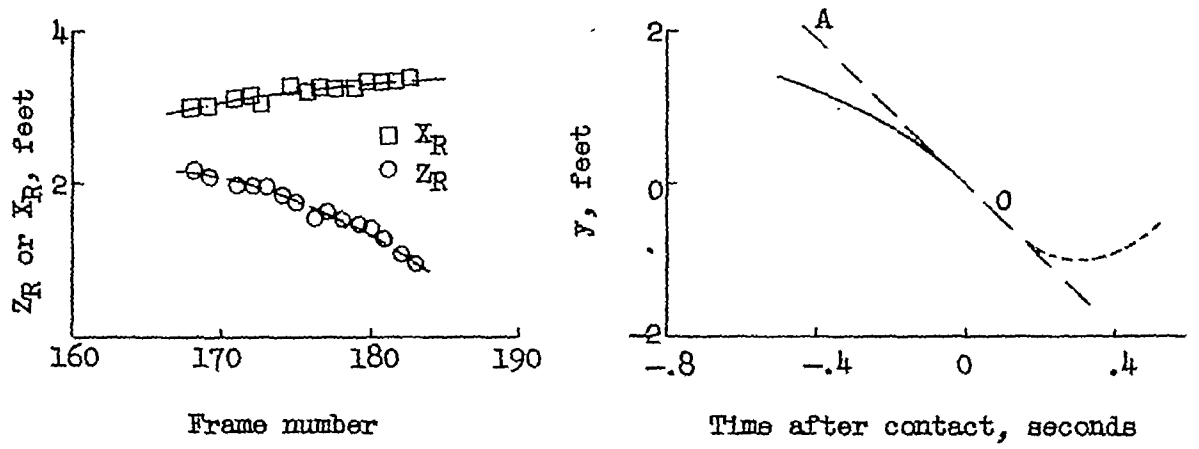

A mean tangent OA was drawn to the curves representing displacement before and after contact. In this case, the vertical velocity at contact was rather difficult to determine and so the accuracy was of the order of ±10 percent.

Values of X_R and Z_R for use in equations (1) and (2) were read from the curves, shown as dashed lines in the preceeding time histories, that were faired through the experimental data. The scatter in the experimental data resulted from the presence of ripples on the surface of the water. The resultant displacement before contact of the step with the water, obtained by using equation (3), is indicated by the solid-line portion of the curves in the time histories and is actually a faired value.

APPENDIX B

DETERMINATION OF WATER PILE-UP

In order to define the draft y_A at which the water line reached the curved-chine region and the draft y_D at which it passed the chine, the transverse water pile-up was determined for a number of impacts. The comparison of the distance below level water with the actual wetted depth was made for a transverse plane LL' which was 31.6 inches forward of the step and the behavior of the water line in the transverse plane at the step was assumed to be similar.

The cross section of the plane LL' and the location of the gages that were mounted at the edge of the V-shape portion of the forebody and at the chine are shown in the following figure:

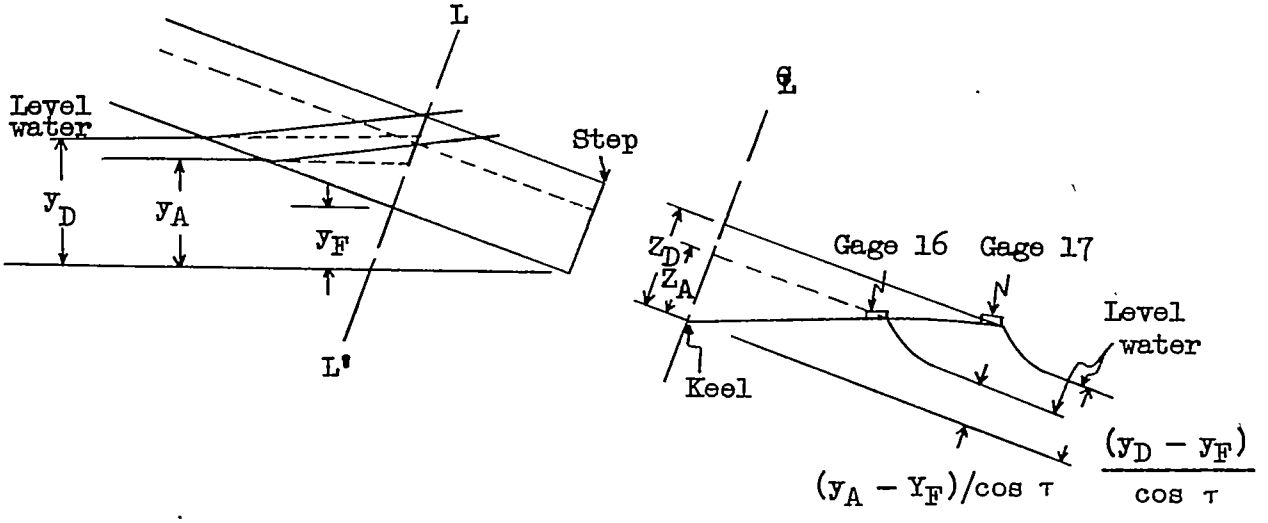

Four additional pressure gages were mounted in this plane at the locations specified in table III. The pressure gages recorded the average pressure acting on a circular area 1 inch in diameter. The high pressures that are associated with the water line clearly identified the travel of the water in the specified plane and along the keel. Plots were made of the wetted beam and the wetted length against time and values were read from each curve at the time that gages 16 and 17 were loaded. The actual drafts y_A and y_D were obtained by multiplying the wetted length l by the corresponding values of $\sin\tau$. The pile-ups then became available as the ratios of the wetted depths $z_A \cos\tau$ and $z_D \cos\tau$ to the corresponding increments of draft $y_A - y_F$ and $y_D - y_F$.

The determination of the pile-up from the time history of the wetted length is given for run 18 for which $\tau = 6.5^\circ$:

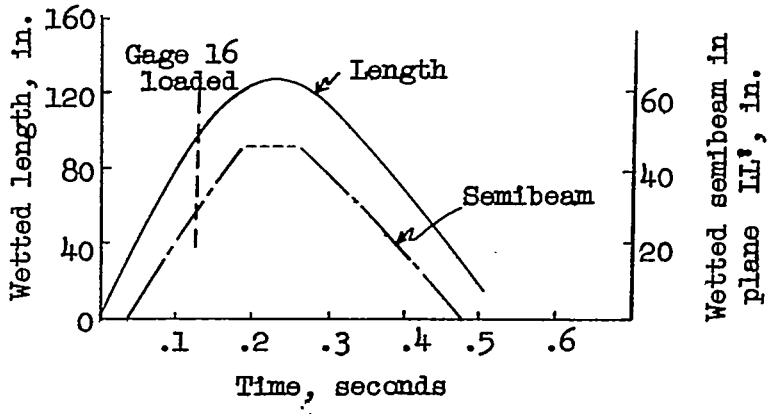

As gage 16 is immersed

$$l = 95 \text{ inches}$$

and

$$c = 29 \text{ inches}$$

therefore

$$y_A = 10.8 \text{ inches}$$

Since $y_F = 31.6 \sin \tau = 3.6$ inches, and $z_A = 10.1$ inches,

$$\frac{z_A \cos \tau}{y_A - y_F} = 1.40$$

The pile-up that occurs when gage 17 is immersed can be determined by the same process where z_D is equal to 14 inches.

The relationship between the wetted beam and the wetted depth is as follows:

$$c = \frac{z_A}{\tan \beta}$$

$$\frac{b}{2} = \frac{\dfrac{y_A - y_F}{\cos \tau}}{\tan \beta}$$

therefore

$$\frac{c}{b/2} = \frac{z_A \cos \tau}{y_A - y_F}$$

REFERENCES

1. Mayo, Wilbur L.: Analysis and Modification of Theory for Impact of Seaplanes on Water. NACA Rep. No. 810, 1945.

2. Milwitzky, Benjamin: A Generalized Theoretical and Experimental Investigation of the Motions and Hydrodynamic Loads Experienced by V-Bottom Seaplanes during Step-Landing Impacts. NACA TN No. 1516, 1948.

3. Milwitzky, Benjamin: A Theoretical Investigation of Hydrodynamic Impact Loads on Scalloped-Bottom Seaplanes and Comparisons with Experiment. NACA TN No. 1363, 1947.

4. Benscoter, Stanley U.: Impact Theory for Seaplane Landings. NACA TN No. 1437, 1947.

5. Milwitzky, Benjamin: A Generalized Theoretical Investigation of the Hydrodynamic Pitching Moments Experienced by V-Bottom Seaplanes during Step-Landing Impact and Comparisons with Experiment. NACA TN No. 1630, 1948.

TABLE I

GENERAL INFORMATION ABOUT FLYING BOAT USED IN FLIGHT TESTS

Normal gross weight, pounds	19,000
Approximate flying weight during tests, pounds	20,000
Stalling speed (flaps down), knots	56
Wing span, feet	86
Wing root chord, feet	11.5
Mean aerodynamic chord, feet	9.8
Wing area, square feet	780.6
Center-of-gravity position,	
percent mean aerodynamic chord	31.9
feet from bow	18.6
Beam of hull, feet	8.33
Distance from main step to bow, feet	21.25
Moment of inertia, slug-feet square	48,137

TABLE II

SPECIFIC LOCATION OF INSTRUMENTS

[See figure 3]

Instrument	Type	Location in airplane (Referred to c.g. or point of step)
1	NACA optical-recording three-component accelerometer	6 in. forward, 3 in. below, 8 in. to starboard from c.g.
2	Inductive-type accelerometer	4 in. forward, 3 in. below, 6 in. to starboard from c.g.
3	Gyroscopic trim recorder	12 in. aft, 60 in. below, 20 in. to port from c.g.
4	NACA airspeed recorder	185 in. forward of step, on top of fuselage on center line
5	NACA optical trim recorder	190 in. forward of step, on top of fuselage, 3 in. to starboard of center line
6	Wing camera	30 in. forward, 146 in. above, 409 in. to starboard of point of step
7	Vertical-displacement indicator	Pivot 13.2 in. aft, 4.4 in. above, 4 in. to port of point of step
8	Water-speed pressure gage	15 in. forward, axis parallel to keel, 11 in. to starboard of point of step
9	Pressure gages	(See table III.)
10	Water-contact indicator (forebody)	Point of step

TABLE III

PRESSURE-GAGE LOCATIONS

[See figure 3; all measurements are made to the center of the pressure gage]

Gage	Longitudinal distance forward from step (in.) (a)	Normal distance from base line (in.)	Transverse distance from keel center line (in.)
1	215.0	6.4	2.5
2	188.0	2.3	2.2
3	162.8	.7	2.2
4	149.8	.5	2.2
5	122.4	.5	2.2
6	92.5	.5	2.4
7	92.5	5.8	17.0
8	92.5	11.7	32.0
9	92.5	13.8	43.5
10	81.5	.5	2.2
11	58.6	.5	2.2
19	31.1	.5	2.5
13	31.1	2.2	7.2
14	31.1	4.0	12.0
15	31.1	5.8	17.0
16	31.1	9.9	28.5
17	31.1	13.8	43.2
18	18.8	.5	2.2
12	-5.5	5.3	2.2
20	-77.8	15.4	2.2
21	-131.0	22.9	2.2
22	-176.0	29.2	2.2

[a]Step reference is 255 inches from bow. All longitudinal measurements made parallel to base line, which is shown in figure 2.

TABLE IV

WATER-CONTACT LOCATIONS

[See figure 5]

Contact	Longitudinal distance forward from step (in.) (a)	Normal distance from base line (in.)	Transverse distance from keel center line (in.)
1	239.0	15.2	12.0
2	230.5	15.2	11.8
3	210.0	19.1	22.5
4	198.0	3.9	6.0
5	187.5	17.9	35.2
6	182.5	14.4	25.5
7	175.2	2.7	6.5
8	154.0	9.9	22.5
9	139.0	2.2	7.5
10	126.5	8.0	22.5
11	116.2	2.2	7.5
12	112.0	13.2	39.0
13	93.5	2.2	7.5
14	93.5	7.7	22.5
15	75.5	2.2	7.5
16	73.5	7.7	22.5
17	54.5	2.2	7.5
18	52.5	7.7	22.5
19	45.5	7.7	22.5
20	38.2	2.2	7.5
21	29.5	13.8	42.8
22	24.8	7.7	22.5
23	17.4	2.2	7.5
24	2.5	2.0	8.8
25	2.5	8.4	24.5
26	-2.5	6.5	7.5
27	-17.3	14.1	22.5
28	-24.7	10.0	7.5
29	-40.5	17.4	22.5
30	-48.5	13.0	7.5
31	-66.3	21.0	22.5
32	-74.2	16.6	7.5
33	-92.0	24.6	22.5
34	-100.0	20.2	7.5
35	-119.0	27.9	22.5
36	-128.0	23.6	7.5
37	-142.0	29.1	23.0
38	-151.0	26.1	6.8
39	-170.0	28.1	2.8

[a]Step reference is 255 inches from bow. All longitudinal measurements made parallel to base line, which is shown in figure 2.

TABLE V

LANDING CONDITIONS

Run	τ_o (deg)	V_{v_o} (ft/sec)	V_{h_o} (ft/sec)	ω_o (deg/sec) (a)	Wing lift at contact (g)	Airspeed (ft/sec)	Impact
1	3.6	1.1	126	-0.7	1.0	126	2
2	5.7	1.4	106	-1.7	1.0	119	2
3	6.2	7.5	83	-9.2	.8	98	3
4	7.1	1.2	105	0.3	1.0	123	1
5	7.2	.9	110	1.8	1.0	121	1
6	7.4	1.0	113	1.2	1.0	120	1
7	7.6	1.3	112	1.0	1.0	119	1
8	7.7	2.0	105	-4.9	.8	114	2
9	8.2	1.4	95	-1.7	1.0	112	1
10	8.4	2.1	103	2.6	1.0	117	1
11	5.2	4.0	99	-3.5	.7	103	2
12	5.4	4.0	106	0	1.0	125	1
13	5.7	3.5	90	-4.7	.8	112	2
14	6.0	4.5	83	-2.8	.7	95	3
15	6.0	4.6	95	-4.9	.8	98	2
16	6.2	3.25	110	0	.9	126	1
17	6.4	3.25	89	-1.1	.8	103	2
18	7.4	6.5	102	-4.2	.9	108	1
19	7.5	3.5	96	-4.4	.8	104	2
20	7.8	6.3	94	-2.6	.9	103	2
21	8.1	3.25	82	-3.0	.7	97	3
22	3.0	9.1	98	-6.0	.8	112	2
23	5.7	7.5	94	-5.0	.8	101	2
24	9.9	3.25	80	-13.0	.8	101	2
25	10.0	4.1	79	-16.0	.7	98	2
26	10.1	1.9	94	-8.0	.9	110	1
27	10.1	2.8	91	-9.0	.9	103	2
28	10.1	3.0	89	-12.9	.9	112	2
29	10.7	2.9	93	-13.0	1.0	110	1
30	10.8	2.4	80	-8.0	.8	98	3
31	10.9	2.9	88	-11.0	.8	103	2
32	11.4	4.0	89	-15.8	.9	101	2

[a]Negative values indicate decreasing trim; positive values indicate increasing trim.

TABLE VI

VARIABLES USED IN COMPUTING THEORETICAL COEFFICIENTS

Run	τ_o (deg)	V_{v_o} (ft/sec)	γ_o (deg)	κ	$n_{i_{w_{max}}}$ (g)	τ_p (deg)	Symbols as represented in figure 8
1	3.6	1.1	0.50	7.18	0.16	3.3	
2	5.7	1.4	.75	7.55	.215	4.7	
3	6.2	7.5	4.82	1.18	1.46	5.2	
4	7.1	1.2	.68	8.77	.184	7.1	
5	7.2	.9	.47	15.14	.13	7.7	○
6	7.4	1.0	.51	14.33	.15	7.3	
7	7.6	1.3	.66	11.36	.25	7.8	
8	7.7	2.0	1.10	6.92	.40	8.9	
9	8.2	1.4	.85	9.3	.27	9.2	
10	8.4	2.1	1.41	5.85	.34	10.0	
11	5.2	4.0	2.31	2.23	1.03	5.1	
12	5.4	4.0	2.16	2.48	.93	5.5	
13	5.7	3.5	2.23	2.53	.93	4.4	
14	6.0	4.6	3.10	1.91	1.21	6.0	
15	6.0	4.5	2.77	2.14	1.16	5.7	□
16	6.2	3.25	1.69	3.63	.93	7.5	
17	6.4	3.25	2.09	3.02	.98	7.3	
18	7.4	6.5	3.64	1.99	1.80	7.0	
19	7.5	3.5	2.09	3.53	1.12	7.4	
20	7.8	6.3	3.83	1.99	1.94	7.3	
21	8.1	3.25	2.27	3.50	.96	7.0	
22	3.0	9.1	5.30	.57	1.85	2.8	△
23	5.7	7.5	4.56	1.23	1.61	5.2	
24	9.9	3.25	2.33	4.32	.91	6.3	
25	10.0	4.1	2.97	3.27	.92	5.5	
26	10.1	1.9	1.15	8.72	.68	7.1	
27	10.1	2.8	1.76	5.59	1.17	7.5	□
28	10.1	3.0	1.92	5.12	1.05	7.0	
29	10.7	2.9	1.79	5.80	.94	6.9	
30	10.8	2.4	1.71	6.13	.84	6.4	
31	10.9	2.9	1.89	5.59	1.08	6.9	
32	11.4	4.0	2.57	4.28	.90	6.3	

NACA

TABLE VII

TRANSVERSE WATER PILE-UP

[See appendix B for sample calculation]

Run	Water line passes gage 16					Water line passes gage 17				
	τ (deg)	y_F (in.)	l (in.)	y_A (in.)	$\frac{z_A \cos \tau}{y_A - y_F}$	τ (deg)	y_F (in.)	l (in.)	y_D (in.)	$\frac{z_D \cos \tau}{y_A - y_F}$
3	5.0	2.8	114	9.9	1.42	4.6	2.5	165	13.2	1.30
12	5.5	3.0	104	10.0	1.45	-----	-----	-----	-----	--------
15	5.4	3.0	106	10.0	1.45	5.5	3.0	135	13.0	1.40
18	6.5	3.6	95	10.8	1.40	7.3	4.0	115	14.6	1.31
20	7.5	4.12	86	11.2	1.41	7.1	3.9	118	14.6	1.30
21	7.2	4.0	86	10.8	1.47	7.0	3.9	112	13.7	1.42
22	2.7	1.5	184	8.7	1.40	3.1	1.7	216	11.7	1.40
23	5.2	2.9	109	9.9	1.45	5.3	2.9	139	12.8	1.41
27	7.4	4.1	88	11.3	1.40	-----	-----	-----	-----	--------
29	6.9	3.8	89	10.7	1.46	-----	-----	-----	-----	--------
32	7.2	4.0	90	11.3	1.37	6.6	3.6	118	13.6	1.40

Figure 1.- Amphibian-type flying boat used in landing investigation.

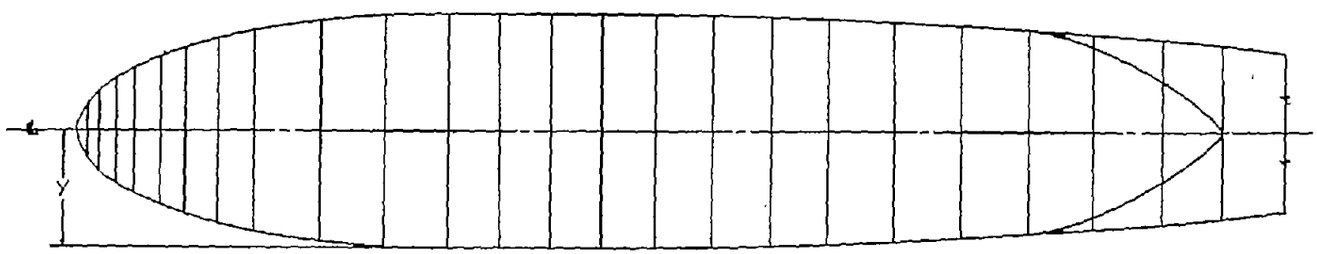

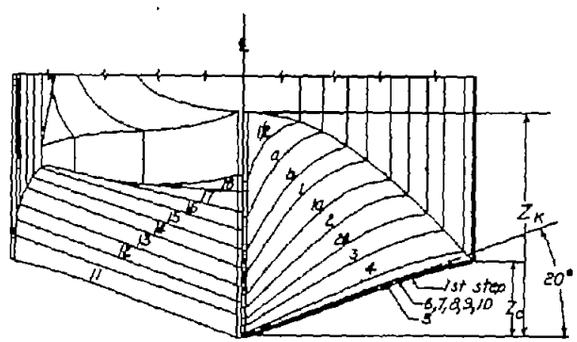

Station	X (in.)	Zk (in.)	Zc (in.)	Y (in.)
0	0	4.30	4.30	.00
1/2	.45	2.56	4.13	1.10
0	5	2.57	3.94	1.53
0	10	1.82	3.28	2.61
1	21	1.18	2.85	3.10
1a	30	.78	2.58	3.43
2	43	.31	2.01	3.91
2a	58	.11	2.16	4.20
3	80	.17	2.05	4.23
4	96	.63	1.85	4.23
5	141	.00	1.53	4.18
6	146	.00	1.42	4.50
7	166	.00	1.32	4.50
8	186	.00	1.40	4.50

Station	X (in.)	Zk (in.)	Zc (in.)	Y (in.)
9	206	.00	1.40	4.50
10	227	.00	1.40	4.48
11	245	-.02	1.35	4.43
at step	255	-.03	1.33	4.42
at step	255	.40	1.93	4.41
12	272	.84	2.57	4.42
13	302	1.57	3.69	4.33
14	330	1.82	4.02	4.22
15	346	1.60	3.84	4.05
16	372	2.05	3.97	3.83
17	397	2.40	3.72	3.20
18	424	2.76	3.96	1.92
19	447	3.10	3.72	.70

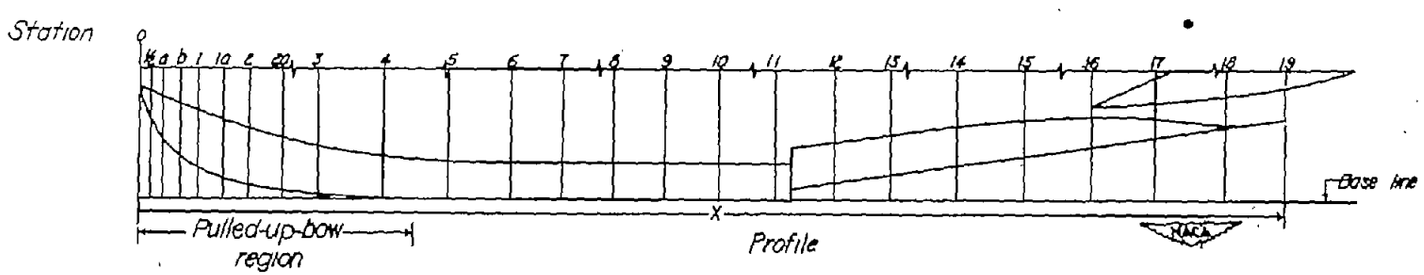

Figure 2.- Hull lines of flying boat used in flight tests.

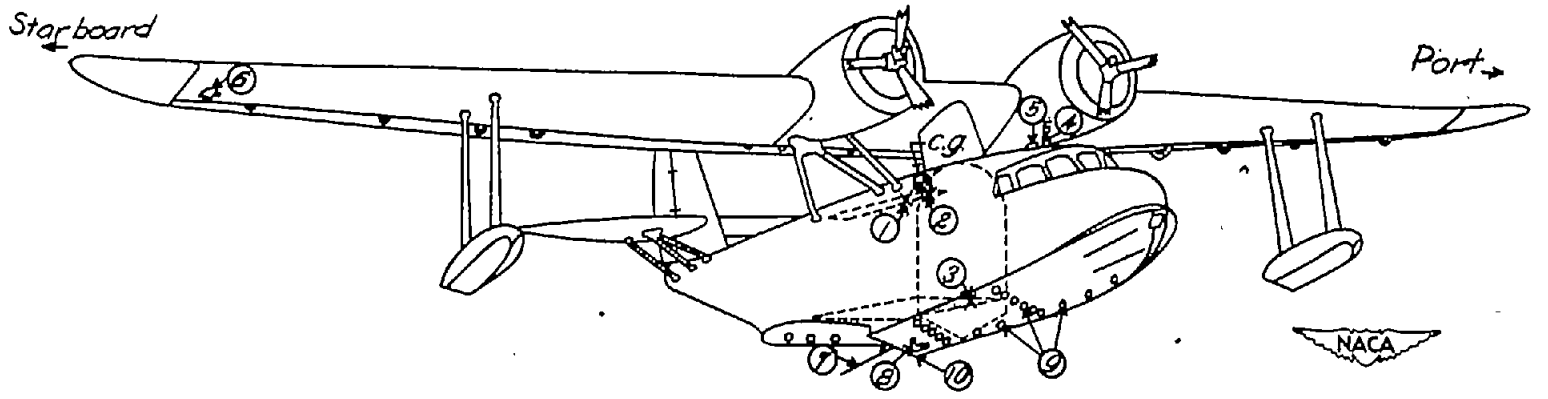

1. NACA optical-recording three-component accelerometer
2. Inductive-type accelerometer
3. Gyroscopic trim recorder
4. NACA airspeed recorder
5. NACA optical trim recorder
6. Wing camera
7. Vertical-displacement indicator
8. Water-speed pressure gage
9. Pressure gages
10. Water-contact indicator (forebody)

Figure 8.- Location of instruments in flying boat.

(a) Water-speed pressure gage.

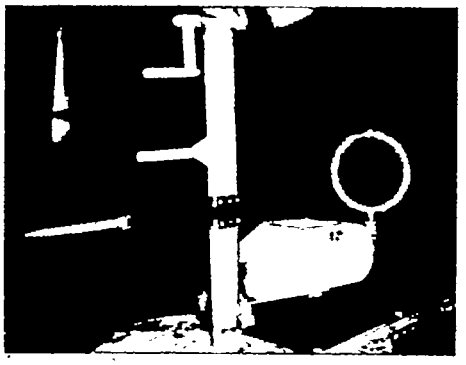

(b) NACA airspeed recorder and NACA optical trim recorder.

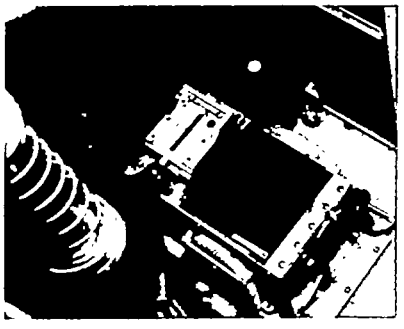

(c) Gyroscopic trim recorder.

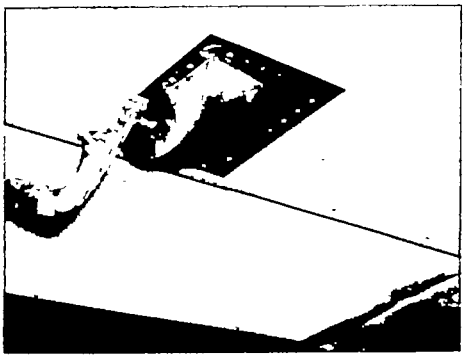

(d) Wing camera.

Figure 4.- Installation of instruments in flying boat.

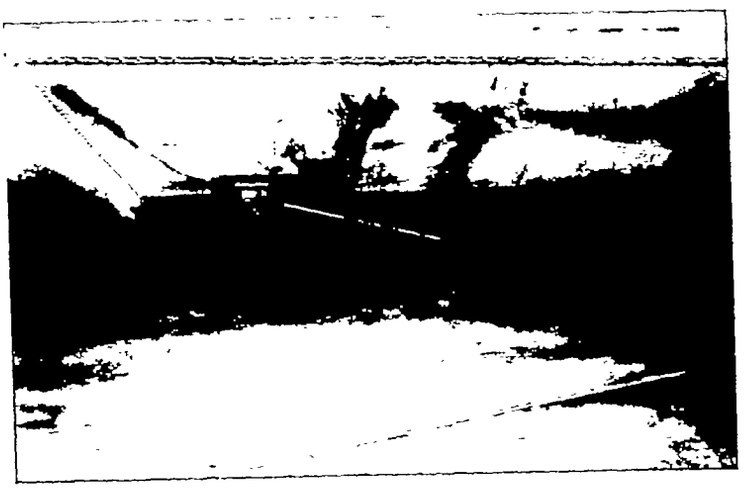

(e) Vertical-displacement indicator.

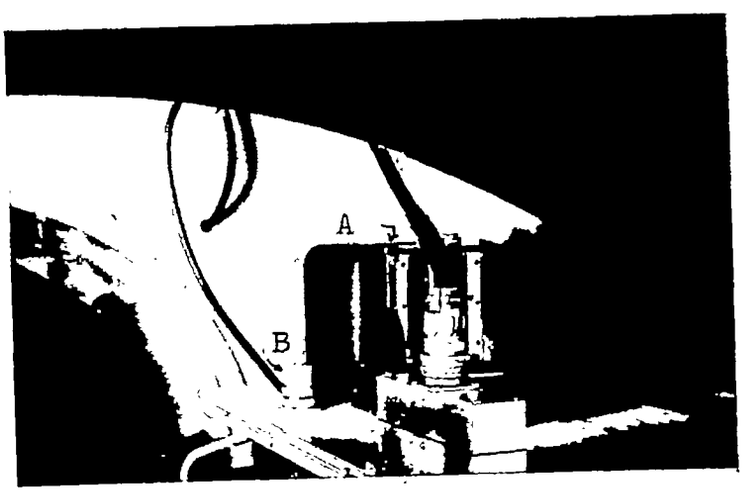

(f) NACA optical-recording three-component accelerometer A and inductive-type accelerometer B.

Figure 4.- Concluded.

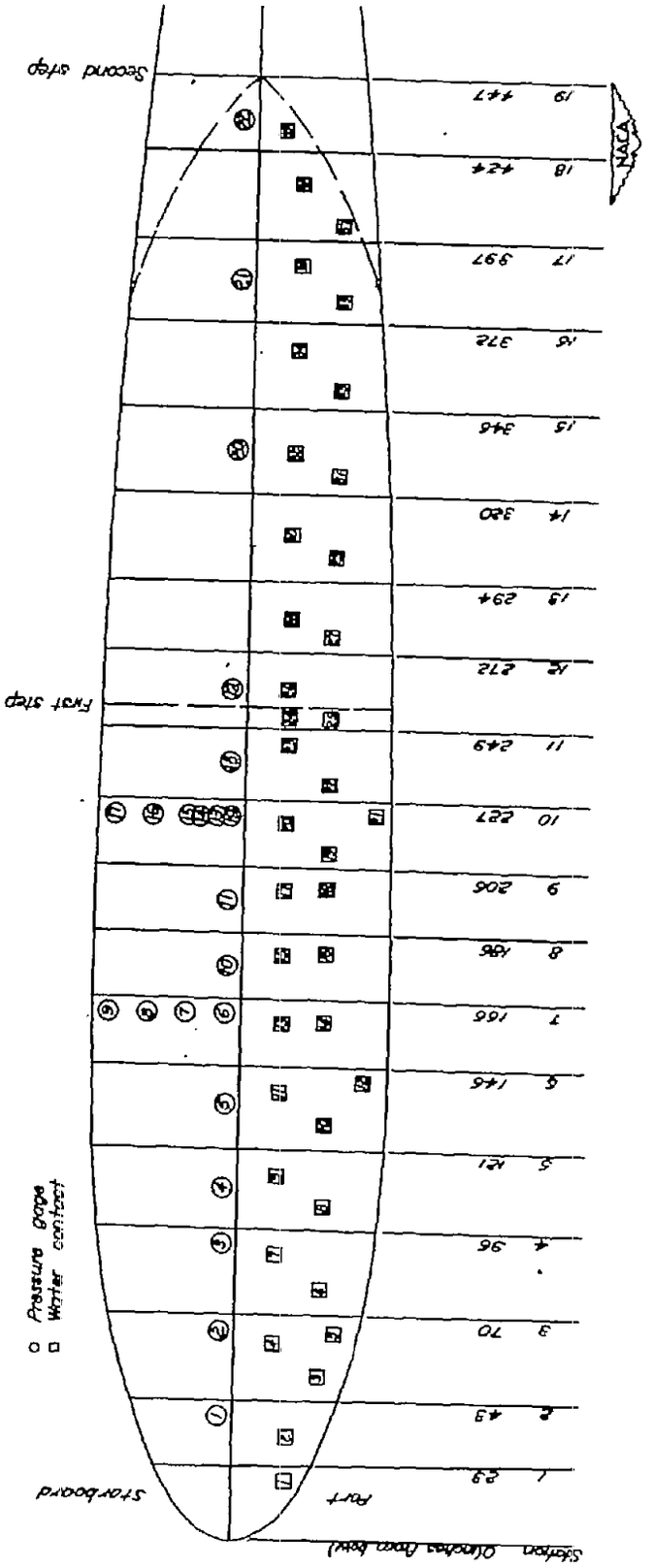

Figure 5.- Location of pressure gages and water contacts in hull bottom.

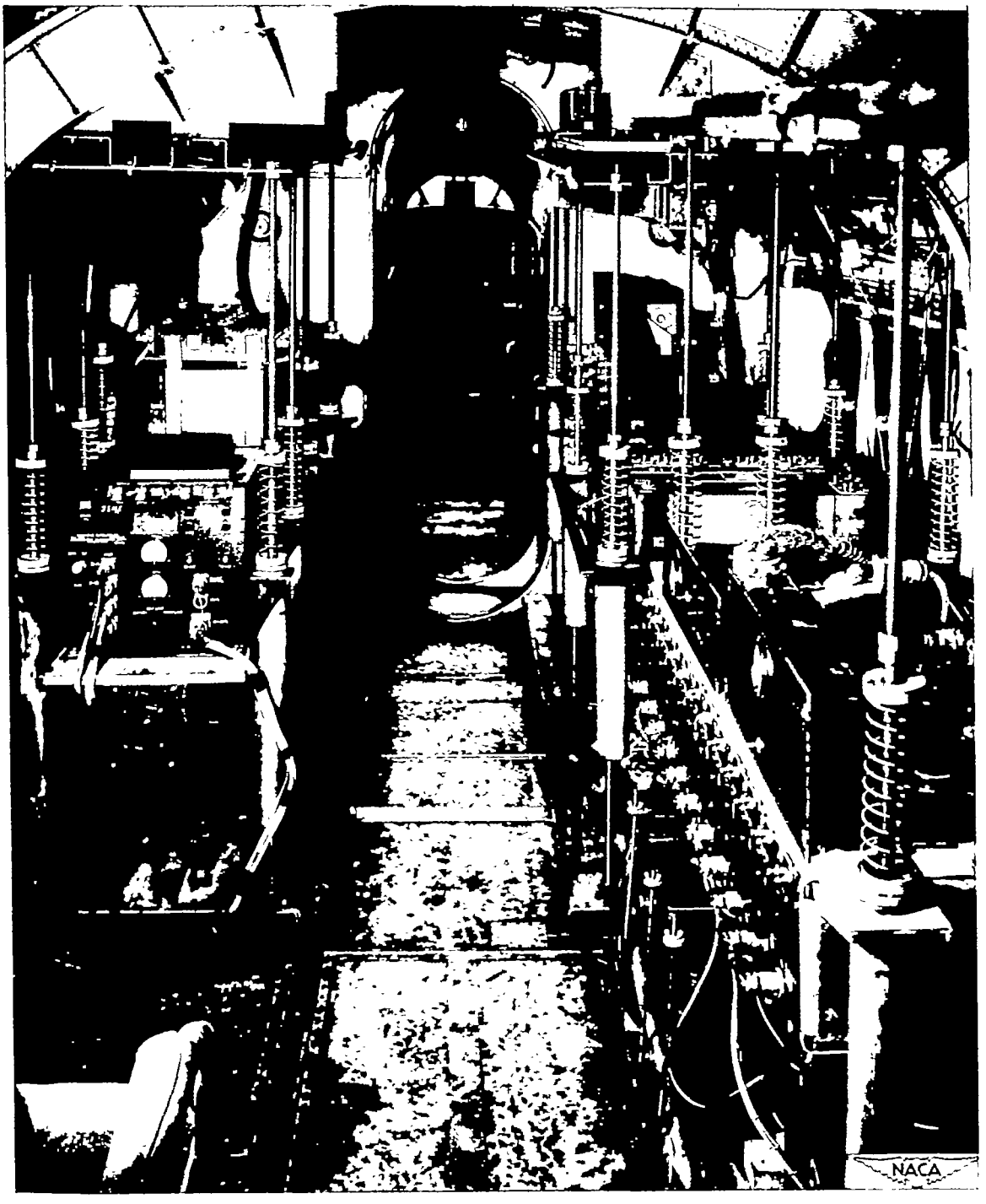

Figure 6.- Installation of amplifying and recording equipment in the main cabin.

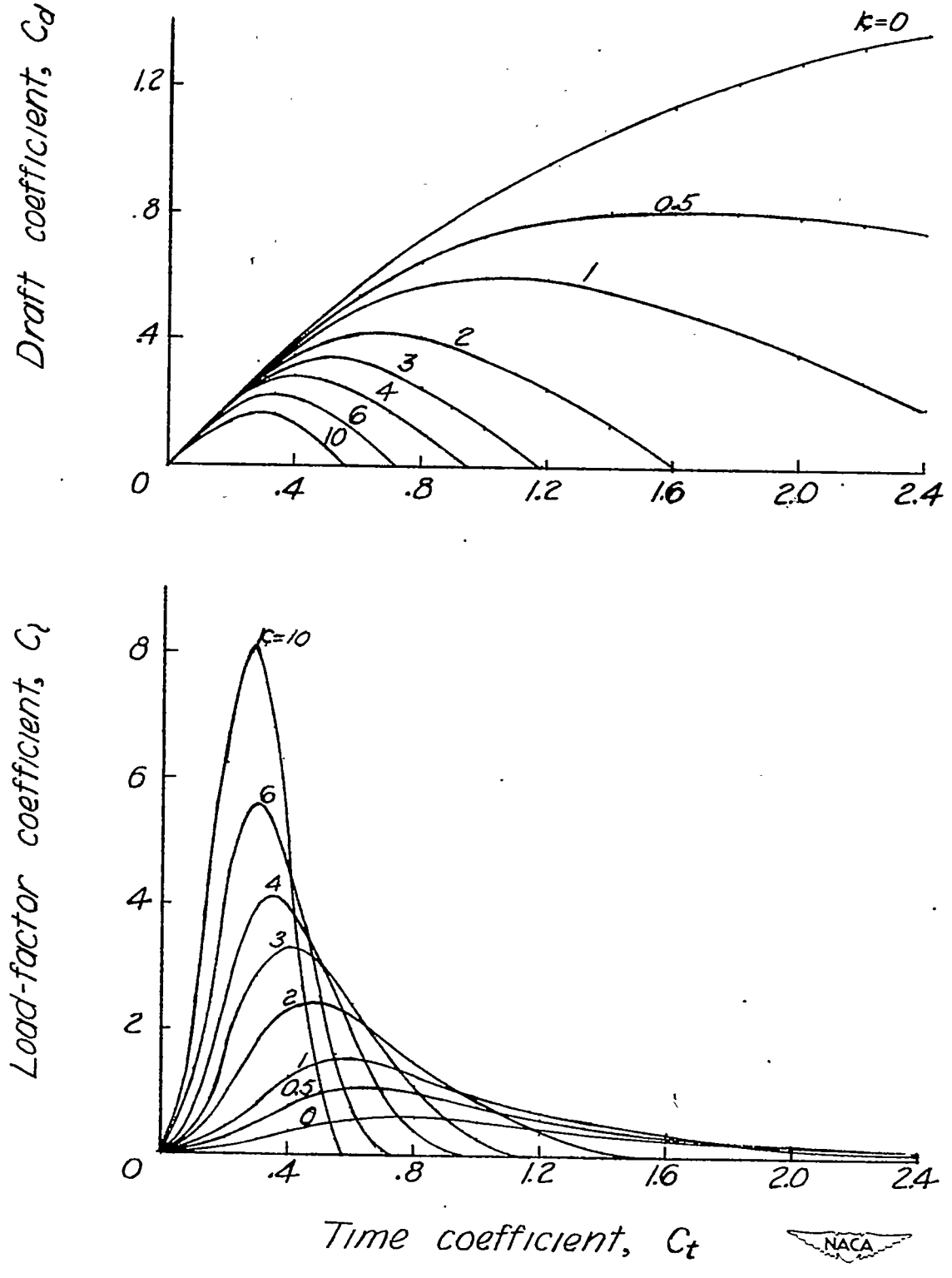

Figure 7.- Theoretical variation of load factor and draft with time. (Reproduced from figures 6 and 8 given in reference 2.)

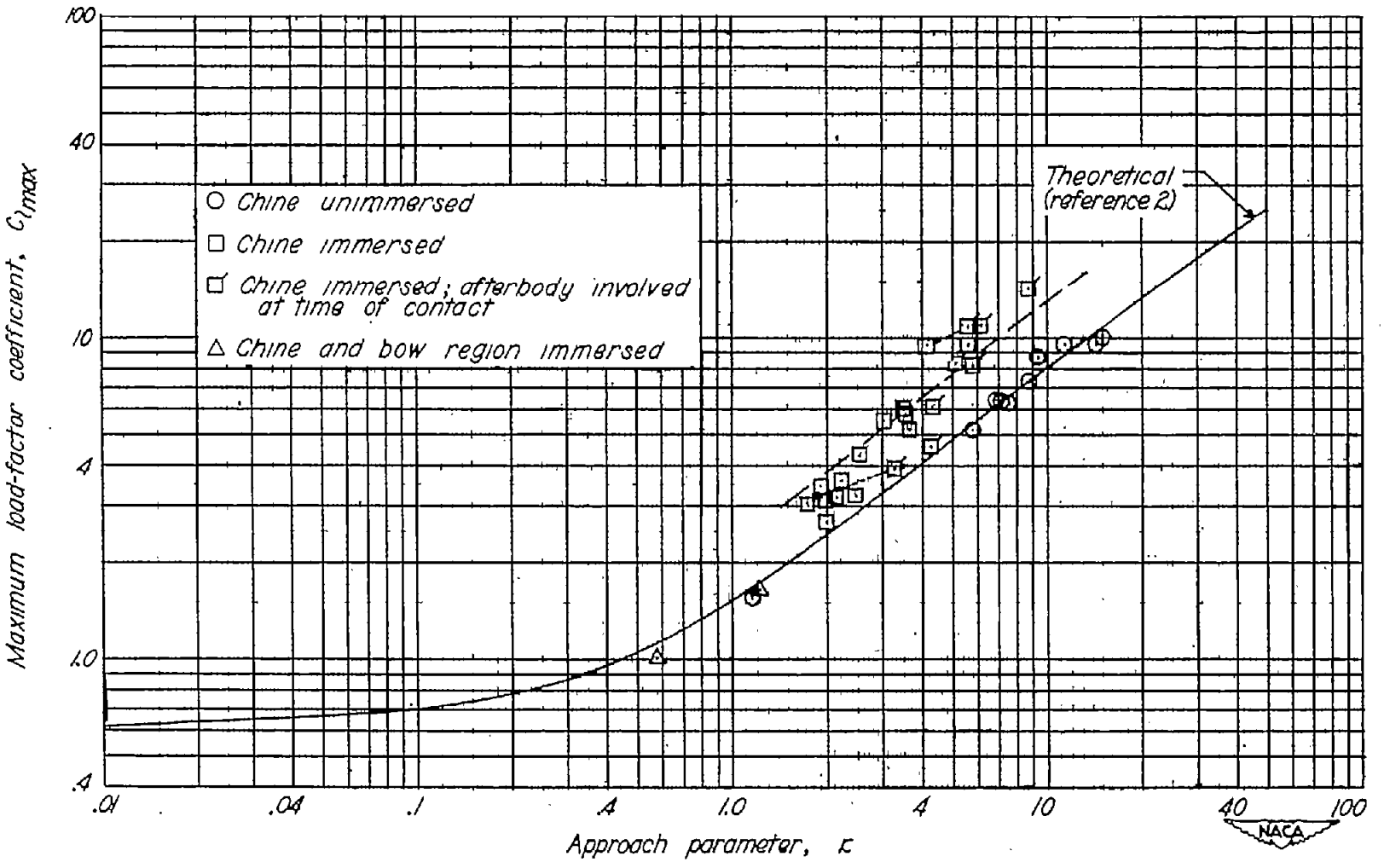

Figure 8.- Comparison of maximum experimental and theoretical load-factor coefficients.

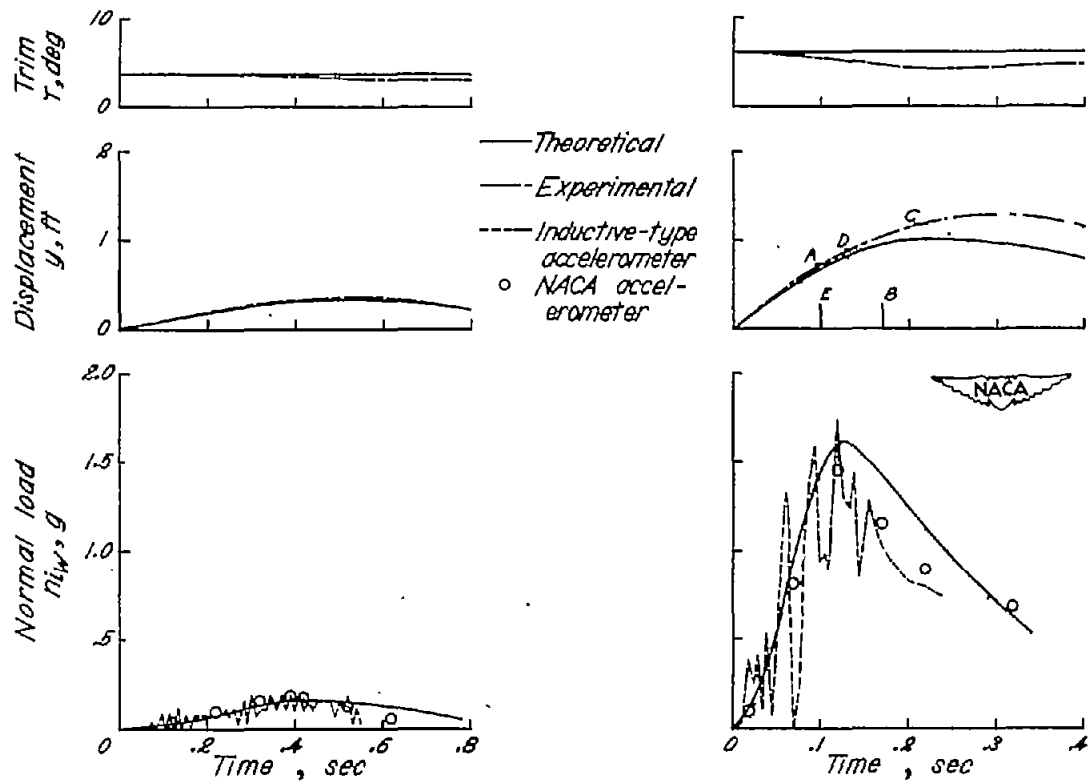

(a) Run 1: V_{v_o} = 1.1 feet per second; V_{h_o} = 126 feet per second; ω_o = -0.7 degrees per second.

(b) Run 3: V_{v_o} = 7.5 feet per second; V_{h_o} = 83 feet per second; ω_o = -9.2 degrees per second.

Figure 9.- Comparison of experimental and computed trims, loads, and displacements. The following notation is used: A, water pile-up reaches curved-chine region; B, pulled-up-bow region enters water; C, level water passes chine; D, water pile-up reaches chine; E, point of application of force reaction is under center of gravity.

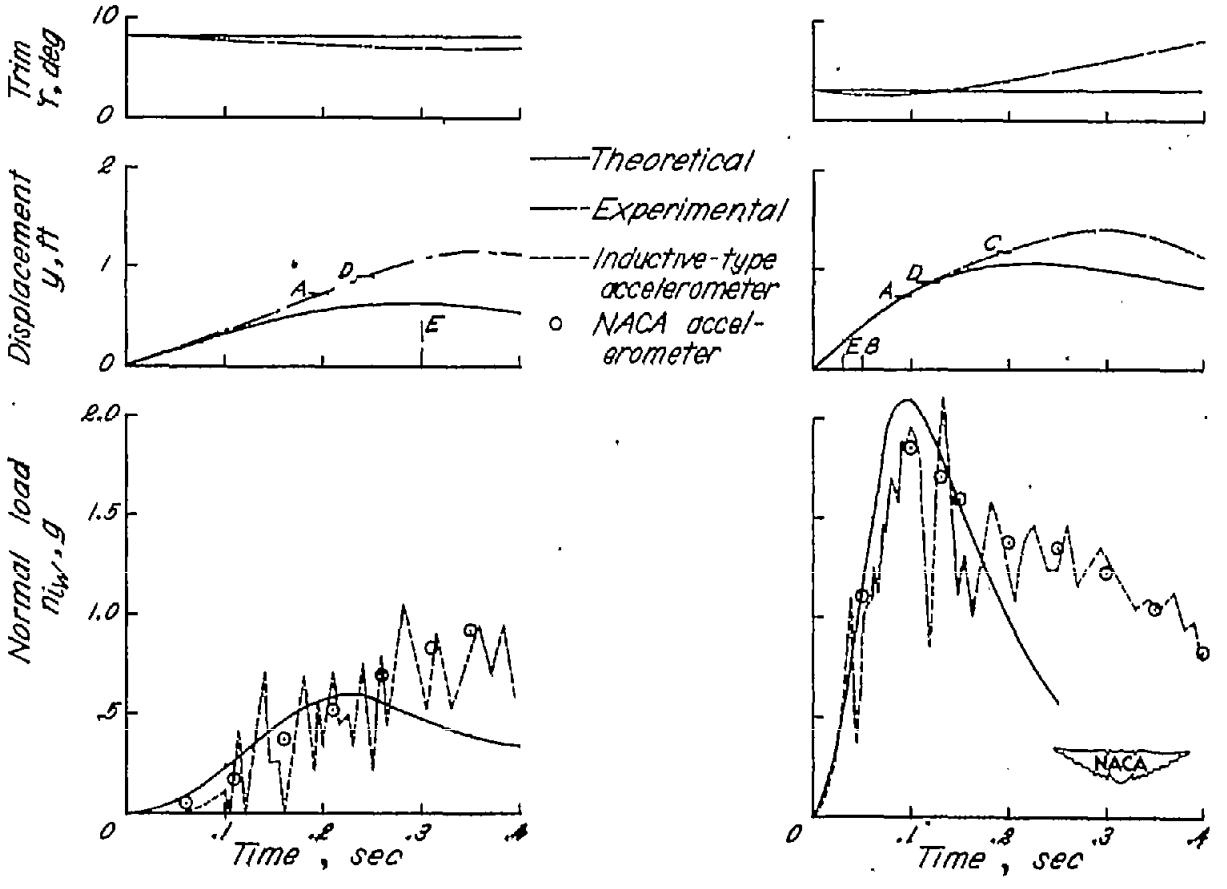

(c) Run 21: V_{v_o} = 3.25 feet per second; V_{h_o} = 82 feet per second; ω_o = -3.0 degrees per second.

(d) Run 22: V_{v_o} = 9.1 feet per second; V_{h_o} = 98 feet per second; ω_o = -6.0 degrees per second.

Figure 9.- Continued.

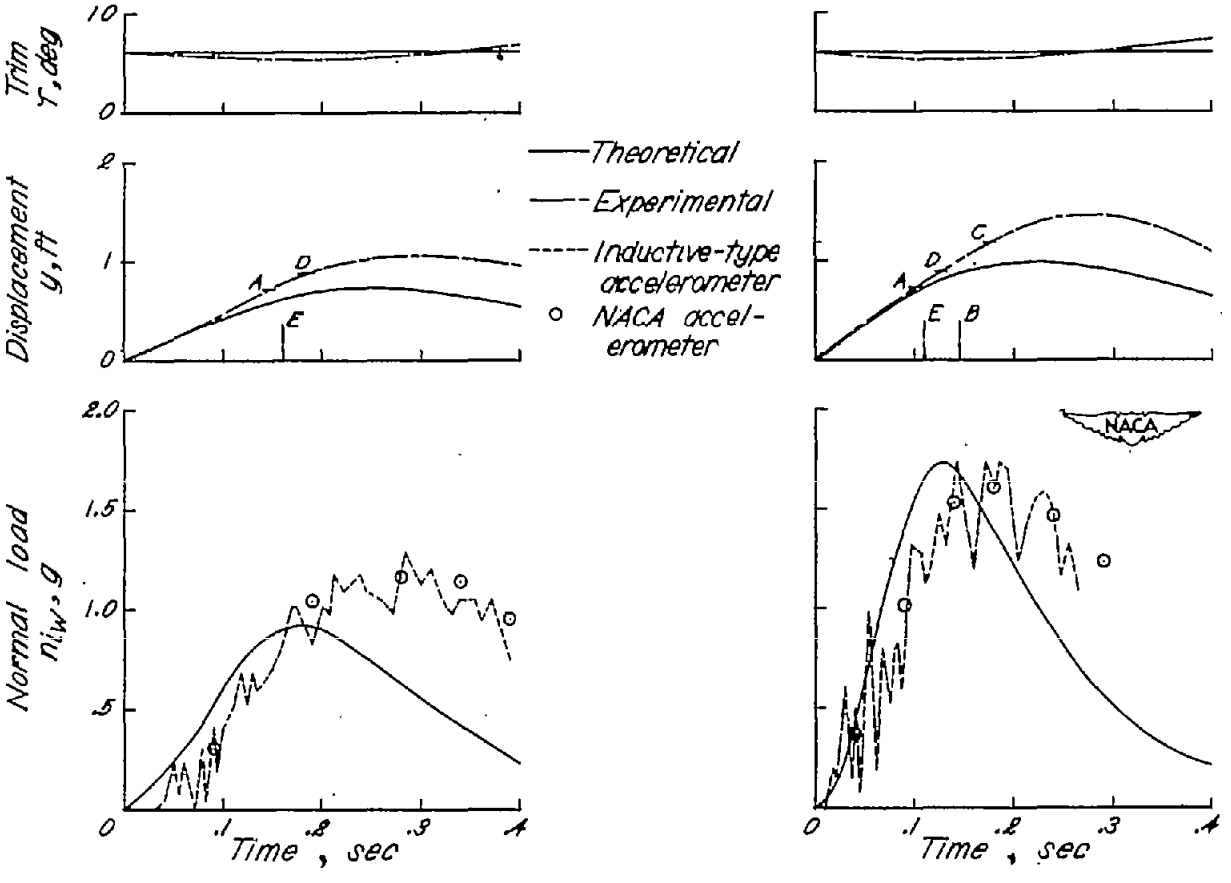

(e) Run 15: V_{V_o} = 4.1 feet per second; V_{h_o} = 95 feet per second; ω_o = -4.9 degrees per second.

(f) Run 23: V_{V_o} = 7.5 feet per second; V_{h_o} = 94 feet per second; ω_o = -5.0 degrees per second.

Figure 9.- Continued.

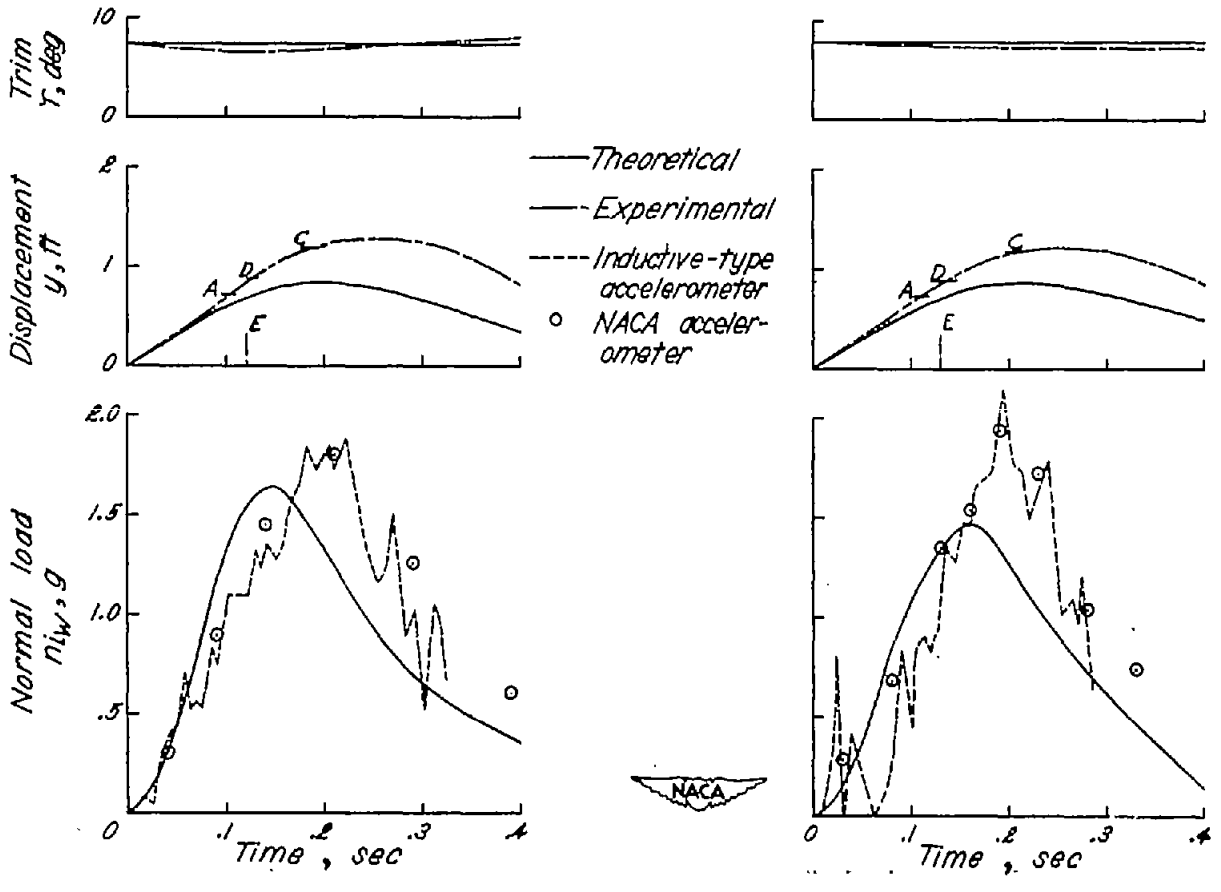

(g) Run 18: V_{v_o} = 6.5 feet per second; V_{h_o} = 102 feet per second; ω_o = -4.2 degrees per second.

(h) Run 20: V_{v_o} = 6.3 feet per second; V_{h_o} = 94 feet per second; ω_o = -2.6 degrees per second.

Figure 9.- Continued.

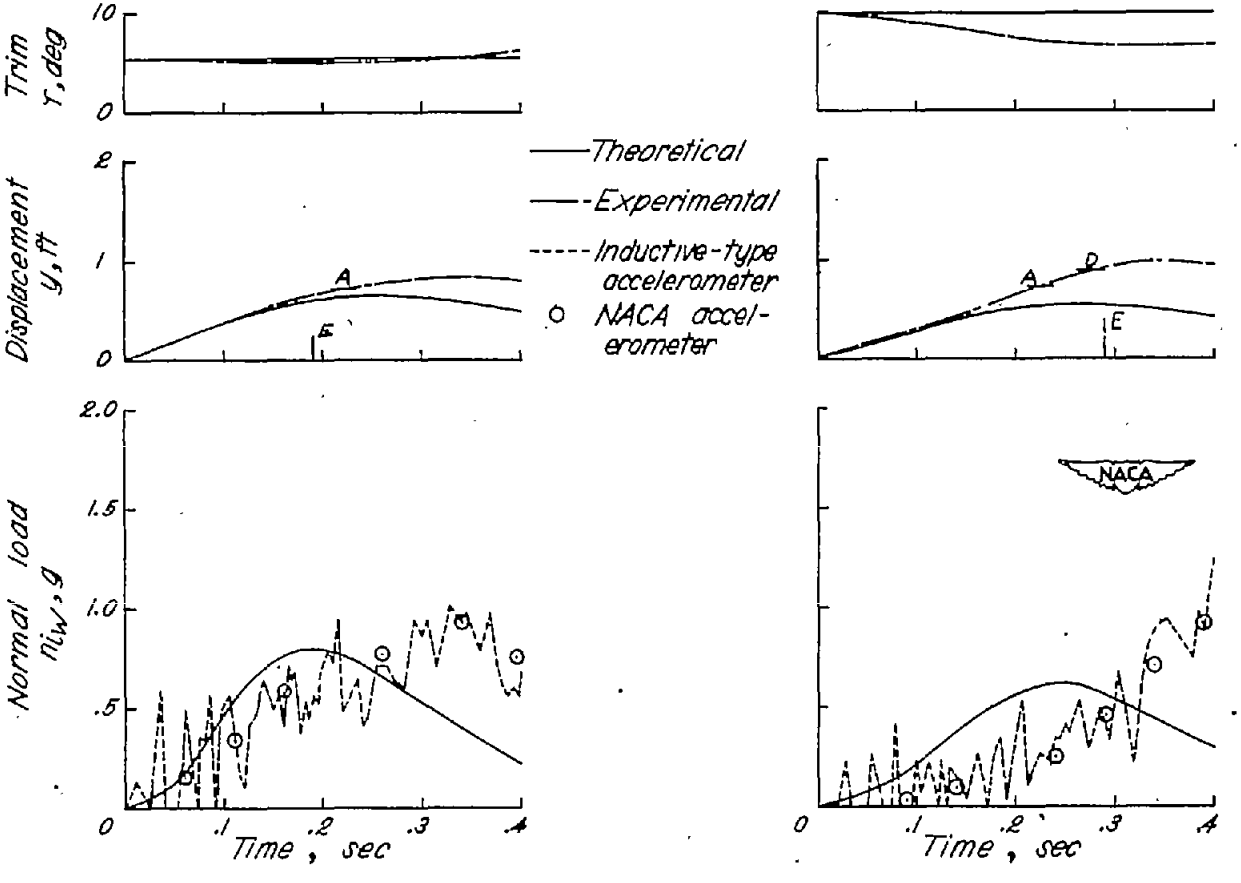

(i) Run 12: V_{v_o} = 4.0 feet per second; V_{h_o} = 106 feet per second; ω_o = 0 degrees per second.

(j) Run 29: V_{v_o} = 2.9 feet per second; V_{h_o} = 93 feet per second; ω_o = -13.0 degrees per second.

Figure 9.- Continued.

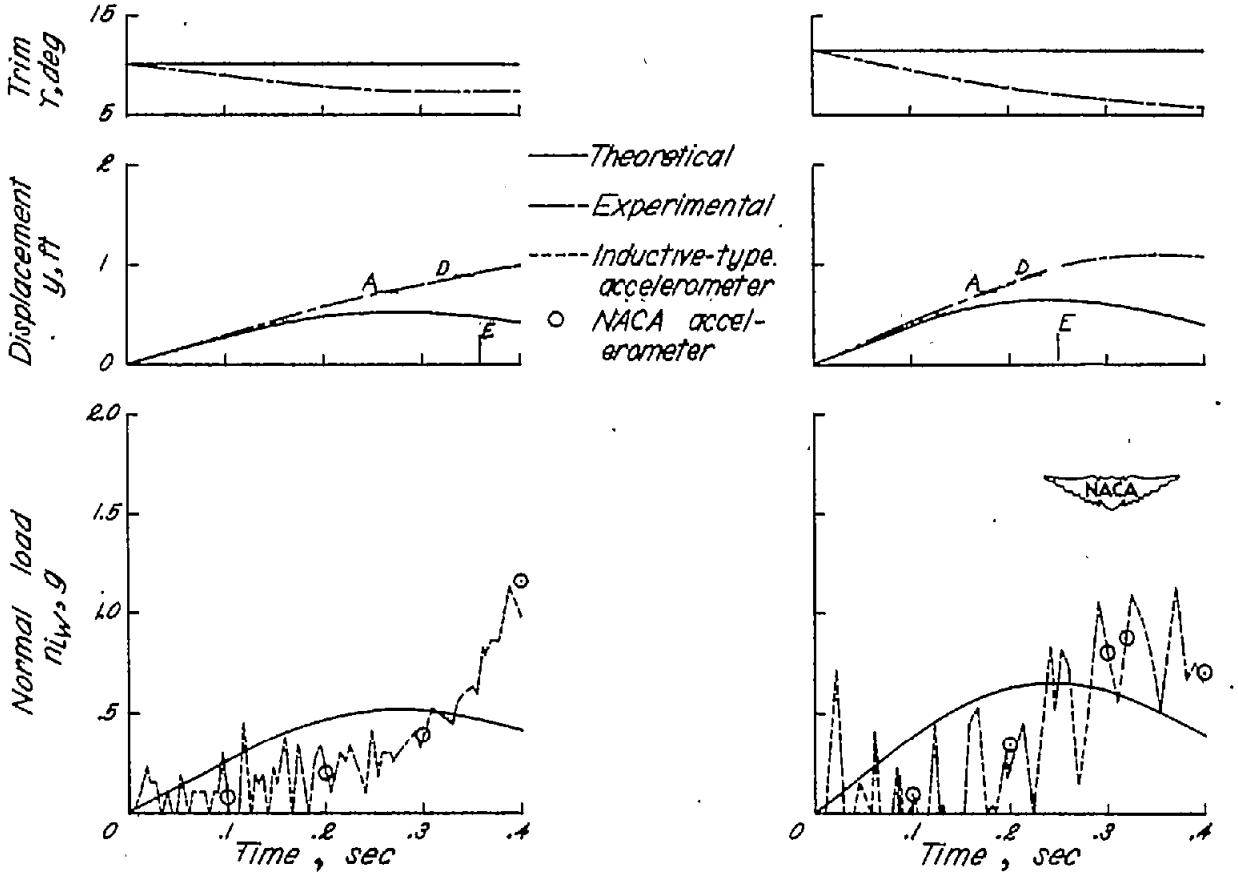

(k) Run 27: V_{v_o} = 2.8 feet per second; V_{h_o} = 91 feet per second; ω_o = -9.0 degrees per second.

(l) Run 32: V_{v_o} = 4.0 feet per second; V_{h_o} = 89 feet per second; ω_o = -15.8 degrees per second.

Figure 9.- Concluded.

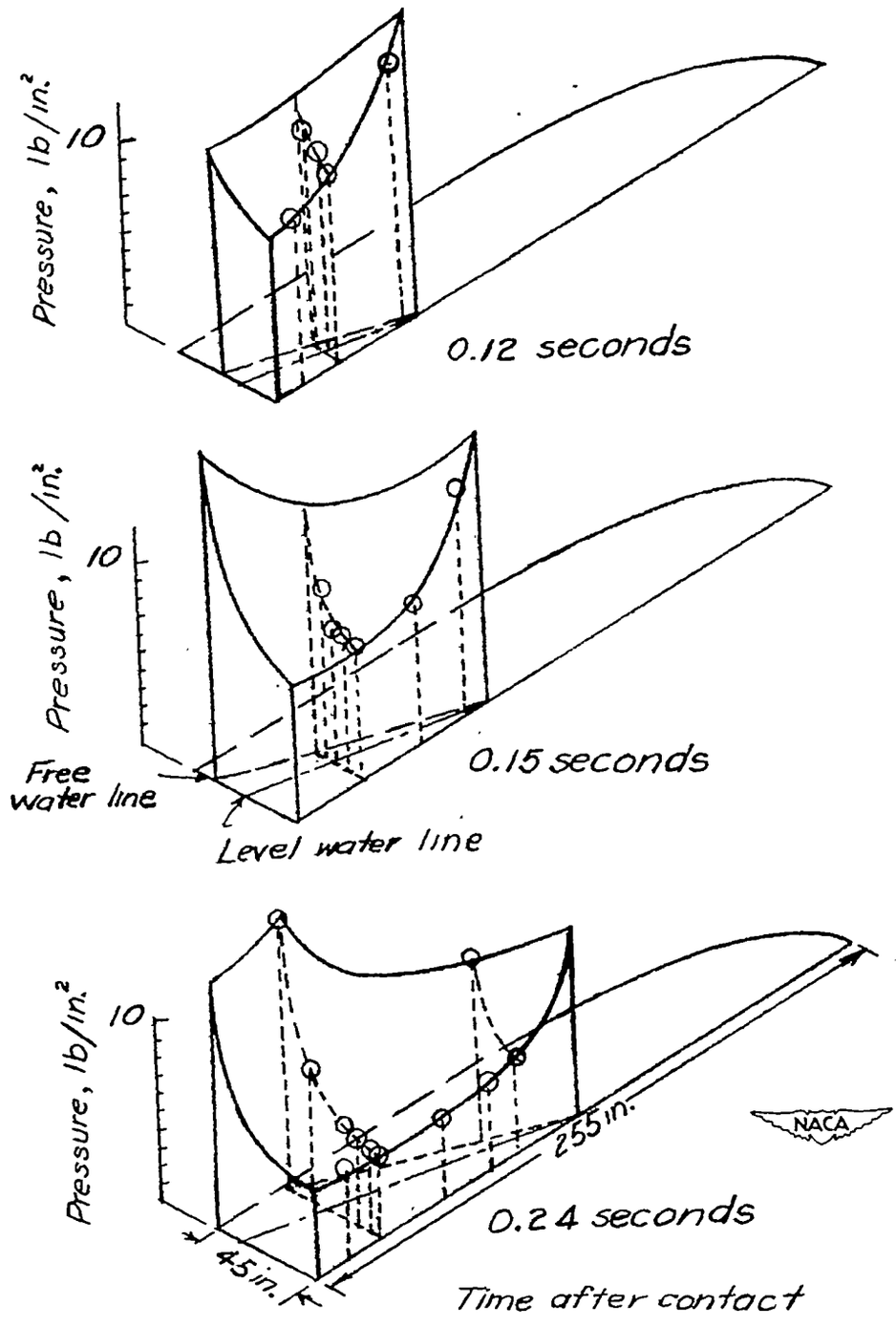

Figure 10.- Pressure distribution on hull bottom during run 15.